2016 24th International Lightning Detection Conference &
6th International Lightning Meteorology Conference
18 - 21 April | San Diego, California, USA

On the Value of Using a 3-axis EB Vector Sensor for Lightning Geolocation

Yongming Zhang, Todor Petrov, Christopher J. Biagi
QUASAR Federal Systems, Inc.
San Diego, CA
yongming@quasarfs.com

Kenneth L. Cummins
Department of Atmospheric Sciences
University of Arizona
Tucson, Arizona

***Abstract*— As part of a recent NASA-sponsored project we studied the feasibility of using a 3-axis electric and magnetic field (EB) sensor to improve the detection of low-altitude and horizontal lightning processes. Operating in the bandwidth from VLF to MF, the elevation angle measured by this sensor is expected to provide better height information for near-ground leader processes than time-of-arrival approaches alone. In particular, it can localize the height above ground with an accuracy of ~20m (for 1 kA effective peak current with the sensor offset 5 km from the event). Given the operating frequency range, this sensor will be capable of reporting fields produced by horizontal and vertical currents associated with k-changes, leader pulses, return strokes, m-components, and associated impulse charge. This project included both analytical and experimental studies. Location accuracy of a network of these sensors was evaluated analytically, coupled with experimentally-derived noise levels. Experimental lightning data were collected at Kennedy Space Center (KSC) during the summer of 2014 using a prototype 3-axis EB sensor. We confirmed that the sensor, once properly configured, will have the required sensitivity, dynamic range and bandwidth for lightning applications with useful sensor baseline distances in the range of 20-100 km. Likely uses of this sensor would be to provide a short-baseline, research-grade Lightning Location System (LLS) composed of these sensors, or to supplement the performance of existing commercial LLS networks with one or more of these sensors to refine measurements at locations of interest. This paper includes a technical description of the sensor, a discussion of analytically-derived performance characteristics, and sample experimental results from the 2014 field measurements referenced to existing KSC lightning measurement systems.**

Keywords—lightning location; sensor

I. INTRODUCTION

The time-of-arrival (TOA) technique is often used by sensor networks to locate lightning processes. A very-short-baseline TOA network consisting of three or more sensors can provide a direction (azimuth and elevation) to a source. The direction information from two such networks can provide location information. TOA networks have provided significant information on lightning development, particularly inside clouds [e.g., Thomas et al., 2004; Cummins and Murphy, 2009].

Although the usefulness of TOA networks has been demonstrated, they can have shortcomings. TOA networks that operate in the VHF range are biased toward processes producing radiation at these frequencies. Moreover, traditional sensors used in TOA networks operate by sensing either the vertical electric field or horizontal magnetic field, which can further restrict the processes that are detected to vertical discharges. As stated above, providing locations using the TOA method requires many sensors. Finally, the location accuracy in the vertical direction tends to be poor for sources near the ground, unless there is a sensor directly beneath the source.

In this paper we discuss a technique to provide direction information on lightning processes using a single sensor that measures all three components of both the electric and magnetic field so that the Poynting vector of the sensed radiation can be computed, and therefore the direction to the source as well. As few as two such sensors can provide a triangulated source location with relatively good accuracy, even for sources close to the ground. In addition to providing a direction vector to a radiating source associated with a lightning process, the sensor measures the horizontal electric field and vertical magnetic field, so it yields more source locations associated with horizontal discharges. Moreover, these field components alone may also provide novel information on lightning processes.

We also discuss the results of a field campaign performed in August and September of 2014 by QUASAR Federal Systems, Inc. (QFS) and the University of Arizona (UA) to test the functionality and operating characteristics of a 3-axis EB vector sensor (henceforth referred to as six-axis sensor) designed specifically for measuring lightning processes. One of the two horizontal electric field sensors was calibrated improperly, which prevented the determination of 3-D locations, but

copious data were collected during the campaign, including horizontal electric field and vertical magnetic field measurements. The field campaign was a first step in an ongoing process of developing a stand-alone sensor that provides a direction vector to an electromagnetic source associated with a lightning process that could be oriented either vertically or horizontally, consist of only low-frequency radiation, and be near the ground.

II. Six-Axis Direction finding

One of QFS's specializations is the development and deployment of compact, integrated six-axis sensors, which measure all six components of the electromagnetic field at a single location. QFS six-axis sensors can be configured with a broadband VLF/LF response and can therefore be used to provide locations for lightning sources produced by current in developed channels. These sensors could be used to construct an independent network that can provide directions via Poynting vector computations in combination with TOA measurements; they could also be used to augment existing TOA networks to improve the accuracy of vertical locations, particularly for sources near ground.

The six-axis sensor used in this study is depicted in Fig. 1. Fig. 1a shows the sensor prototype used for the test. Fig. 1b shows the sensor deployed in the field inside weatherproof Pelican cases. The three electric field components are sensed by two pairs of circular, flat plate electrodes that are oriented orthogonally. The electric field for each horizontal direction is simply the potential difference between the two plates divided by the distance. The vertical electric field is determined by combining the measurements of the two horizontal components (note that each horizontal component is measured at a different height). The three magnetic field components are measured by specially designed induction coils that are oriented orthogonally to each other.

The six components of the electromagnetic field can be used to determine the Poynting vector of the source at the location of the sensor, given by

$$\vec{S} = \frac{1}{\mu_0}\vec{E} \times \vec{B} \tag{1}$$

where μ_0 is the permeability of free space. The components of the k-vector, or the direction of incoming radiation, can be defined by expanding the cross product

$$k_x = E_y B_z - E_z B_y \tag{2}$$

$$k_y = E_z B_x - E_x B_z \tag{3}$$

$$k_z = E_x B_y - E_y B_x \tag{4}$$

The direction to the source is the negative of the radiation k-vector. The accuracy of the direction provided using the Poynting vector calculation depends primarily on the accuracy

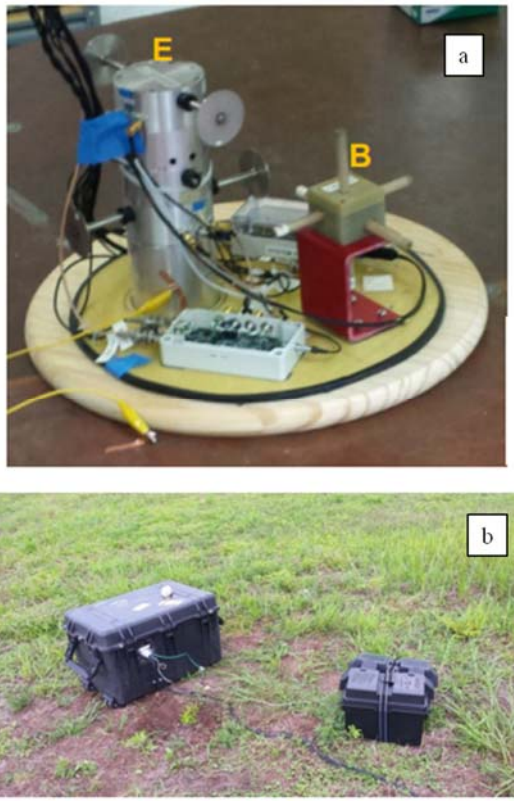

Fig. 1. Pictures of the six-axis sensor.

of the field amplitude measurements. A detailed description of the location error associated with the direction finding of a six-axis sensor is beyond the scope of this paper. However, several possible sources of error can be discussed, including calibration error, site errors, timing errors, and noise errors. It is straightforward to ensure accurate amplitude and phase calibration. Measurements can be compensated to account for effects of site errors on individual field components. Timing errors for a single six-axis sensor are not significant since the incoming wave arrives simultaneously at each component antenna. The sensor is designed such that all six of the component antennas have nearly identical phase responses, and the small phase differences can be calibrated out. Some phase variation may be problematic for measurements of radiation in the near field regime, but when the source is in the far field region, which dominates at ranges beyond about ten kilometers, the electric and magnetic field components are in phase.

If we assume that the sensor is calibrated accurately, that adjustments have been made for site errors, and that errors in amplitude measurements are random (errors in each field vector measurement are independent), then the accuracy can be related to the signal-to-noise ratio (SNR) of the sensor channels. A reasonable estimate can be made of the statistical (i.e., noise induced) direction finding uncertainties based on SNR. The angular uncertainty is given as

$$\Delta\theta \cong \arctan\left(\frac{1}{\mathrm{SNR}}\right) \tag{5}$$

If SNR >> 1, then Equation 5 can be approximated as $\Delta\theta \approx 1/SNR$. For example, if the SNR value is 50 dB, then the theoretical angular uncertainty is about 0.18 degrees. The corresponding directional uncertainty at a range of 10 km is about 32 m in the plane perpendicular to the direction of the k vector. Table 1 lists the angular error for SNRs values between 20 dB and 55 dB.

Table 1. Angular Error Estimates

SNR (dB)	SNR (linear)	Angular Uncertainty (milliradians)	Angular Uncertainty (deg)	Location Uncertainty at 10 km (m)
20	10	100	5.7	1,000
25	18	56	3.2	560
30	32	32	1.8	320
35	56	18	1.0	180
40	100	10	0.57	100
45	180	5.6	0.32	56
50	320	3.2	0.18	32
55	560	1.8	0.1	18

Fig. 2 shows the lab-measured noise spectrum from 1 kHz to 300 kHz for each field component of the six axis sensor used in this study. According to these noise figures, any lightning process that produces at the sensor location an electric field magnitude of about 6 mV/m and a magnetic field magnitude of about 10 nT would be sensed with a SNR of at least 50 dB. Although the noise floor of the sensor will not limit the directional performance of the six-axis sensor, background noise may be problematic. According to the International Telecommunication Union, the rms background noise levels in vertical electric field and horizontal magnetic field between frequencies of 1 kHz and 1 MHz are 20 mV/m and 66 pT, respectively. In order to attain a 50 dB SNR with such levels of background noise, the signal strength of the electric and magnetic field must be about 6 V/m and 21 nT, respectively. These field levels are conservative estimates, and it should be noted that there will be significant variations at certain frequencies, such as, for example, typically AM radio frequencies.

III. Sensor Performance Characteristics

A. *Identifying Processes of Interest*

In order to determine a suitable bandwidth, sensitivity, and dynamic range, we identified a subset of lightning processes occurring during cloud-to-ground (CG) and intra-cloud (IC) lightning that might be detectable by the six-axis sensor. Table 2 contains definitions of detection-related parameters for our set of CG and IC processes. The most important characteristic for detectability is the peak source strength, which we converted to an "equivalent peak current" (EPI) in kA. This allows all processes to be characterized by a well-understood measurement unit that is related linearly to the range-normalized radiation peak electric and magnetic field

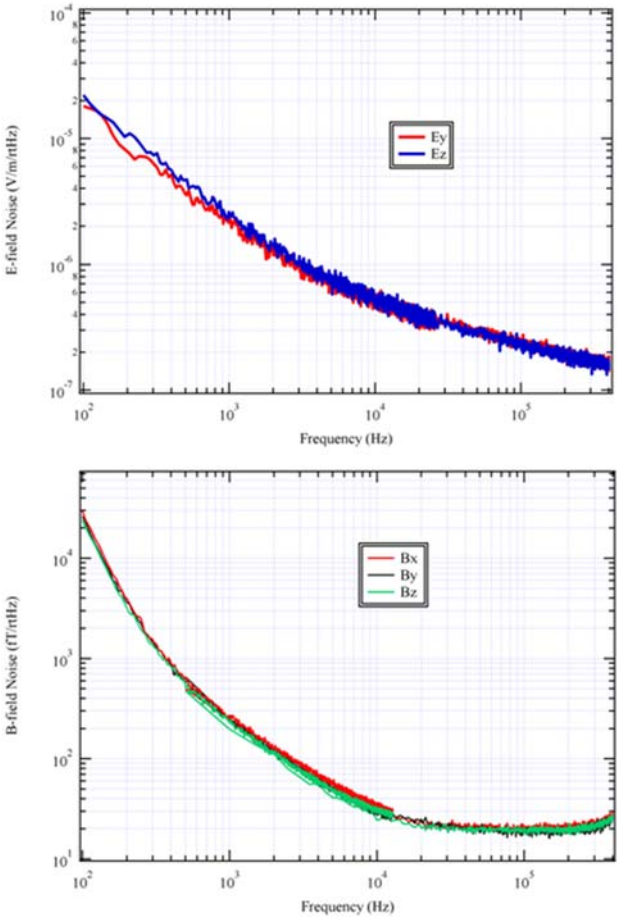

Fig. 2. Sensor noise figures.

strength. This is an oversimplification, since the signals measured at close range will include induction and/or static field components that can be much larger than the radiation field, but in those cases, we tried to include all field components for our EPI estimate. Specifically, the EPI is given by well-known transmission line model, applied to the larger of the electric or magnetic field strengths. This simplification leads to an "amplitude uncertainty" of at least a factor-of-two, but given that all lightning processes have amplitude ranges of more than a factor-of-ten, this uncertainty was deemed acceptable.

Table 2 also contains a "range of heights" (AGL) we identified where the processes of interest generally occur. These heights determine the potential value of 3D geolocation, and the potential difficulty in determining height using remote electromagnetic sensing. When a process occurs over a wide range of heights, the heights of interest are identified in the column "Process-Related Comments."

The remaining process characteristics are related to waveform features. The pulse rise-time and fall-time (in combination with EPI) both play significant roles in determining how accurately the arrival-time of the discharge can be measured. The combined rise- and fall-times determine the upper and lower-frequency requirements if one is to

Table 2. Detection Related Parameters

Lightning Process	Equivalent Peak Current Range (kA)	Range of Heights (km)	Pulse Rise/Fall Times (μs)	Frequency Range	Pulse Temporal Separation
CG: Neg. Preliminary Breakdown Pulses	1 – 100[d,e]	3-6	(1 - 10) / (1 - 10)[d,e]	10 kHz – 500 kHz	70-130 μs
CG: Neg. Downward Stepped Leaders	1 - 100	0.1 – 10	(0.05 - 1) / (0.1 - 1)[f,g]	100 kHz – 5 MHz	1-25 μs
CG: Return Stroke and Impulse Charge	0.5 - 300[a,c]	0	(0.25 - 10) / (10 - 2000)	200 Hz - 1 MHz	0.02 - 500 ms[a,b,c]
CG: Continuing Current	0.01 – 2[d]	0	15 to 500 ms	1 Hz - 1 kHz	N/A
CG: M-Components	0.02 – 1	0	(0.1 - 1) / (0.2 - 2)	200 Hz – 20 kHz	0.8 – 23 ms
CG: Near-Ground Horizontal RS Channel	TBD	TBD	TBD	TBD	TBD
CG: Near-Ground Horizontal Branches	TBD	TBD	TBD	TBD	TBD
CG: In-Cloud Horizontal Breakdown	TBD	TBD	TBD	TBD	TBD
CG: In-Cloud Horizontal High-Current Channels	TBD	TBD	TBD	TBD	TBD
IC: Initial Breakdown Pulses	0.1 – 10	4 – 10	(1 – 20) / (1 – 20)	10 kHz – 500 kHz	0.6 – 0.8 ms
IC: Neg. Leaders Toward Pos. Charge	0.5 – 10	5 – 15	TBD	~10 kHz – 2 MHz	TBD
IC: High-Current Vertical Channel Currents	1 – 30	4 – 10	TBD	~10 kHz – 1 MHz	0.1 – 500 ms
IC: In-Cloud Horizontal Breakdown	TBD	TBD	TBD	TBD	TBD
IC: In-Cloud Horizontal High-Current Channels	TBD	TBD	TBD	TBD	TBD

[a] Stolzenberg et al. (2012)
[b] Kong et al. (2009)
[c] Campos et al. (2014)
[d] Nag and Rakov (2005)
[e] Nag et al. (2009)
[f] Willett et al. (1990)
[g] Howard et al. (2011)

measure faithfully the processes (reflected in the frequency range listed in the table). Finally, the pulse temporal separation determines practical constraints on the identification and measurement of closely-spaced pulses that might occur for a given process.

A review of the frequency range "characteristic" in Table 2 indicates that most processes of interest can be measured faithfully within a bandwidth of 200 Hz to 1.0 MHz. The low-frequency exception is continuing current, which would require a low frequency limit no greater than 1 Hz. The high-frequency exceptions are the negative leaders, which would likely require an upper-frequency limit of 2-5 MHz to measure properly. Note that the frequency limits are somewhat smaller than those employed in the quoted references, and reflects expected trade-offs due to expected sensor separation distances and faithful signal reproduction.

The discussion of Table 2 thus far has been limited to what is known about using the "traditional" horizontal magnetic field (B_h, composed of north-south and east-west components) and the associated Vertical electric field (E_z). As discussed earlier in this report, the QFS six-axis sensor is capable of measuring the vertical magnetic field (B_z) and the horizontal electric field (E_h, composed of north-south and east-west components). The E_h components originate from elevated vertical sources and all horizontal sources, and can therefore provide useful information about channel geometry near the ground. Additionally, E_h is a direct source for coupling voltage and current transients onto horizontal conductors on the ground. The magnitude and shape of the horizontal E-field waveforms are altered by the soil electrical conductivity down to several meters. Thomson et al. (1988) studied the horizontal electric field for CG return strokes at KSC, and found that the waveform looked much like the time-derivative of the vertical electric field, with peak values on the order of 3-4% of the vertical field. In our requirement for minimum E_h, we employed the scaling of 3% found by Thomson et al.

There is no body of information about the behavior of B_z produced by nearby lightning. On theoretical grounds, we know that the horizontal channels and elevated current sources will produce vertical magnetic fields, much like what occurs for horizontal electric fields. Additionally, the magnetic field does not suffer from the conductivity boundary at the earth's surface, so larger B_z magnitudes can be expected than are seen for E_h. We note that magnetic fields produced by near-ground horizontal discharges above a launch site, such as side branches

of return-stroke channels, may produce larger EMC-related problems than the associated electric fields, depending on conductor geometric and shielding. Given the uncertainties discussed above, our detection requirement for B_z needs to be studied.

B. Sensor Design

After considering the requirements presented in Table 2, we applied high-pass filters to each sensor component to reduce the likelihood of digitizer saturation from the induction and static components of nearby discharges. The magnetic field outputs were high-pass filtered using a single pole filter with a 3 dB frequency of 10 kHz, and the electric field outputs were high-pass filtered using a multi-pole filter beginning at 1 kHz. A total of 56 dB of dynamic range was required to measure the full range of EPI values, between 500 A to 300 kA, and adding 25 dB of SNR increased the dynamic range requirement to 81 dB. Thus, we used a 16-bit digitizer having an upper sampling rate of 800 kS/s. In order to prevent aliasing, the low-pass filters were applied to the electric and magnetic field sensors with 3-dB points of 300 kHz and 400 kHz, respectively. It is worth noting that the requirements in dynamic range could be relaxed for a multiple-sensor network owing to the fact that although a lightning discharge may saturate a nearby sensor, it would not saturate a more distant sensor. Fig. 3 shows a block diagram of the finalized sensor setup.

IV. Example Data

In this section we present some example data acquired with the six-axis sensor during a field campaign at the Kennedy Space Center from 14 August to 23 September, 2014. After the field campaign, it was discovered that one of the two horizontal electric field sensors had malfunctioned and provided inaccurate amplitude values, so unfortunately no 3-D locations were obtained. However, many thousands of waveforms of lightning processes associated with intra-cloud and cloud-to-ground lightning were obtained, including vertical magnetic field measurements.

A. Signal Restoration

In an effort to manage the dynamic range requirements during this measurement campaign (as described above) the three B-field channels included a single-pole high-pass filter with a break frequency of 10 kHz, resulting in a signal that represents the time- derivative for frequencies below about 8 kHz. The E-field channels included a multi-pole high-pass filter at 1000 Hz. In order to compensate the recorded waveforms for inter-comparison down to about 300 Hz, we employed a signal restoration procedure that "re-integrated" the signal at low frequencies. Examples of "raw" and restored horizontal magnetic field (B_x and B_y) and vertical electric field (E_z) signals for a 37 kA negative CG return stroke at a distance of 137 km are shown in Fig. 4. In both cases, the DC offsets were removed and gain calibrations were applied prior to plotting. The left vertical axis is in nT (nano-Tesla) for the magnetic

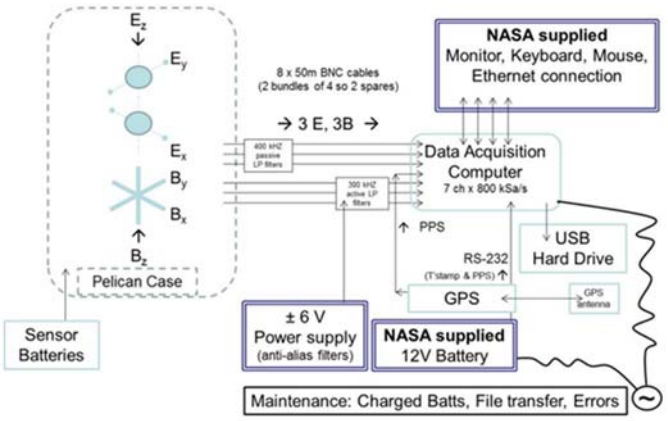

Fig. 3. Block diagram of sensor.

field waveforms. The right vertical axis is in V/m for the electric field signals. The relative scales of the two axes are set such that the E-field waveform peak will be equal to the RMS magnitude of the B_x and B_y peaks if the electric field were perfectly calibrated and the signals were a pure radiation fields (distance to lightning > ~20 km). Note that the non-restored signals have a zero-crossing that occurs within about 30 μs after the major peak, whereas the restored signals have identical zero-crossing times that occur more than 100 μs after the peak. This period reflects the duration of the impulse charge for this event.

B. Correlated NLDN and Waveform Analysis

In this section we provide a comparative analysis between the waveform data and NLDN-reported CG strokes near the test site. We describe the method used to correlate the datasets, and then we discuss findings related to field strength vs. range, azimuth error, and error in arrival-time measurements. The reference dataset for this analysis is all

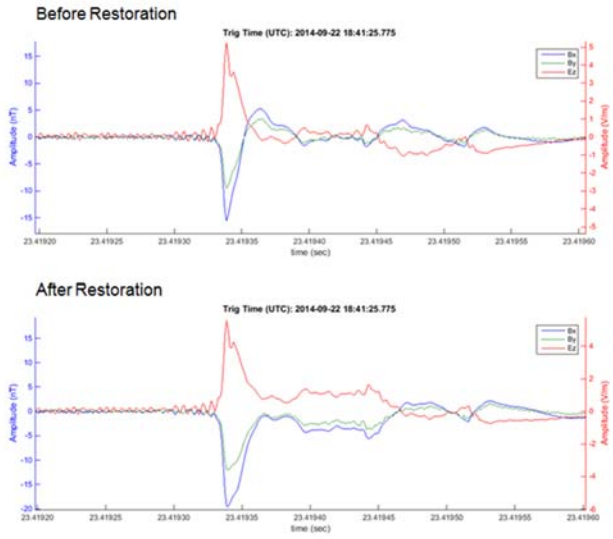

Fig. 4. Example of waveforms with restored low-frequency content.

NLDN-reported CG strokes in the range of 10 to 200 km from the test site between September 12 and 23, 2014. Relevant NLDN parameters were the stroke time to the microsecond, estimated peak current in kA, arrival angle (degrees positive from north), and distance to the stroke in km. All waveform data files during this time period (over 15,000) were reviewed to determine whether they contained a NLDN-reported CG stroke within 200 km of the site. If so, the NLDN stroke time and distance were used to compute arrival times at the test sensor, with an expected accuracy of about +/- 2 μs. The time-correlated waveforms were then inspected to determine waveform-based arrival time (halfway between the waveform onset and its peak) to a precision of about 1 μs, and the peak amplitude for each channel. From these data, we were able to determine the waveform-based peak amplitude of the horizontal magnetic field and the arrival angle.

Our findings are shown in Fig. 5. The timing error is shown in histogram form. Although depicted as an error, this is simply the timing difference between the NLDN stroke time (adjusted for propagation distance, with an uncertainty of about +/- 2 μs) and the waveform arrival time. Given that our test sensor's timing resolution is limited by the 800 kHz sampling rate (used to determine the GPS PPS time), the range and shape of this histogram is quite reasonable. The behavior of the sensors horizontal B amplitude vs. range is shown in scattergram form, including a power-law fit. According to the Transmission Line model, the exponent for this fit should be -1.0. For these data the exponent is -0.93 with 90% of the variance being accounted for in this fit ($R^2 = 0.901$). This result is also quite good. Finally, the sensor angle error is also depicted as a scattergram, with the waveform-derived azimuth (from B_x and B_y) plotted as a function of the NLDN-derived azimuth. Given that local site errors have not been calculated or applied to these data, the waveform-derived azimuth is quite good. The data point color in this figure represents the magnitude of the horizontal magnetic field in Volts. The few widely-scattered points generally occur for low-amplitude events.

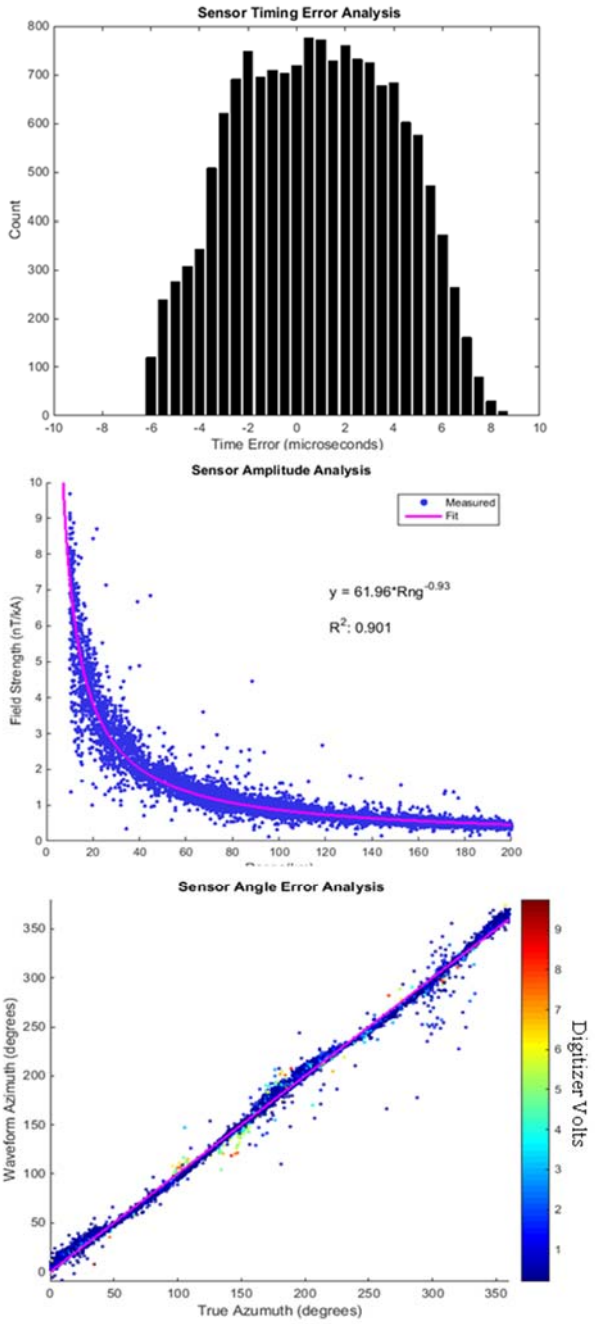

Fig. 5. Sensor performance from comparison with NLDN reports.

C. Cloud-to-Ground Case Studies

In the preceding sections of the report we have demonstrated the general behavior of the sensor. The cloud-to-ground cases provided below were selected to explore the behavior of the vertical magnetic field (B_z) for CG-related lightning processes that are known to occur at different heights.

In this section, we present waveforms measured at close range (<30 km) that include (1) Preliminary Breakdown (PB) pulses that start at heights in the range of 4-5 km, (2) near-ground stepped leaders that occur at height of less 2 km above ground, (3) the early front of return-stroke waveforms that occur within a few hundred meters of ground, and finally (4) the falling edge of return-stroke waveforms that include effects of removing charge from significant channel branches in the lower few km of the channel that were established by the descending leader. All of these processes generally occurred in a 5ms to 50 ms period prior-to and during a return stroke. Although there has been some research regarding the horizontal electric fields (e.g. Thomson et al. 1998 and references therein), little work has gone into studying the vertical magnetic field. We are optimistic that this field component will provide unique information about non-vertical near-ground lightning process that have the potential to create lightning protection problems.

Cases are supported by NLDN CG data and LDAR 3D mapping data, as required. The NLDN data are used to confirm stroke times, locations, and peak current. LDAR data are used

to assess the 3-dimensional location of breakdown processes as a function of time.

a) Case 1: This 6-stroke CG flash occurred at 19:12:01 UTC on September 22. The CG strokes were all located within a few hundred meters of each other according to the NLDN, and at a distance of about 12 km northeast of our sensor. The waveform plot in Fig. 6 shows the three magnetic field component measurements for all six strokes with NLDN estimated peak currents. The first stroke had a peak current of -28.4 kA, but the third stroke was the largest, with a peak current of -64.3 kA. The particularly interesting element of this flash is that from the time of the preliminary breakdown through the beginning of the 3rd stroke, the B_z signal (red) is large and discernible. Following the third stroke, the B_z signal remains near the baseline (zero) value.

The LDAR Time/Height plot in Fig. 7 shows the time evolution of the reported "sources" (associated with electrical breakdown processes) for the duration of the flash. The earliest sources occur at a height of about 6 km, and continue to occur near that height for tens of milliseconds. Following this time period, a stepped-leader apparently travels toward the ground with a fairly constant speed and connects to ground at 19:12:01.434. Since there are no additional downward leaders apparent in the LDAR data during the rest of the flash, it is likely that the remainder of the return strokes occurred in the main vertical channel produced by the stepped leader and first return stroke. LDAR data, which provided full 3-dimensional information about this flash, indicate that the stepped leader path appears to have traveled about 1 km horizontally before descending towards the ground. Fig. 8 shows the preliminary breakdown waveforms (upper) and near-ground stepped leaders (lower) prior to the first stroke of this flash. Although the B_z field strength is large during the final leader phase at the beginning of the RS, it is much smaller than either B_x or B_y during the RS. These findings are exciting and seem qualitatively reasonable. They also indicate clearly that there could be useful information in horizontal magnetic field waveforms. Fig. 9 shows the magnetic field data around the time of the 3rd RS in this flash. This stroke had a peak current of -64 kA at a distance of 12 km, and it saturated the B_x and B_y channels during the rising (negative) edge of the RS, resulting in the bipolar characteristic once the sensor came out of saturation. The third stroke was the last stroke with approximately equally strong B_x, B_y, and B_z signals (see Fig. 6) for approximately 200 μs prior to the return stroke. Moreover, it is evident in Fig. 6 that the Bz

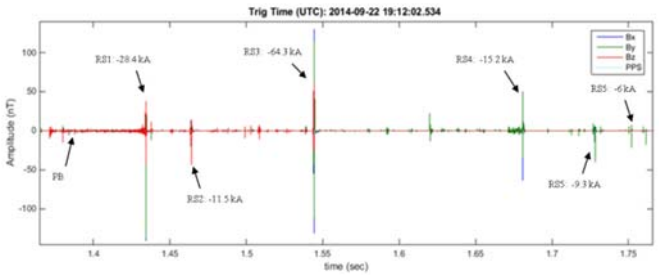

Fig. 6. Measured magnetic field for case 1 CG flash.

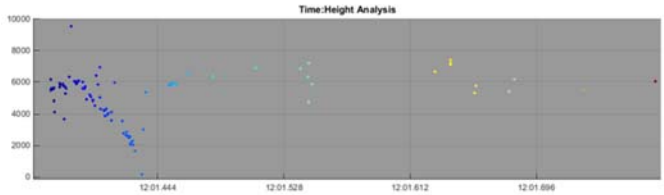

Fig. 7. LDAR data for case 1 CG flash.

signal became significantly smaller in amplitude following the third, and largest peak current, return stroke.

These data indicate that the third return stroke significantly changed the electrical characteristics of the lightning channel, perhaps increasing the electrical conductivity by further "conditioning" it, or perhaps reducing the channel tortuosity and therefore the amount of channel that was oriented horizontally.

b) Case 2: Case 1 was representative of the data for CG flashes occurring within about 12 km of the sensor site. For more distant strokes, the relative B_z magnitude for the leader (compared to B_x and B_y) can still be substantial, but the early return stroke signal gets somewhat smaller at greater distances from the site. This is illustrated in Fig. 10, which shows the preliminary breakdown (top) and return stroke (bottom) portions of a first stroke with a peak current of -65.5 kA and occurring at a distance of 54 km. Note that the leader activity before the return strokes is not well-defined in our data due to the upper frequency limit being 400 kHz.

D. Cloud Flash Case

In this section, we present a representative case of an intra-cloud flash centered at a distance about 20 km from our sensor. According to the LDAR data shown in Fig. 11, this flash had a horizontal extent of about 10 km, and it extended radially from the site to the northeast. The time/height plot in the lower panel can be used to discuss some (simplified) characteristics of a typical cloud flash as they relate to signals reported by our sensor. The flash began with an initial breakdown pulse at a height of about 6 km.

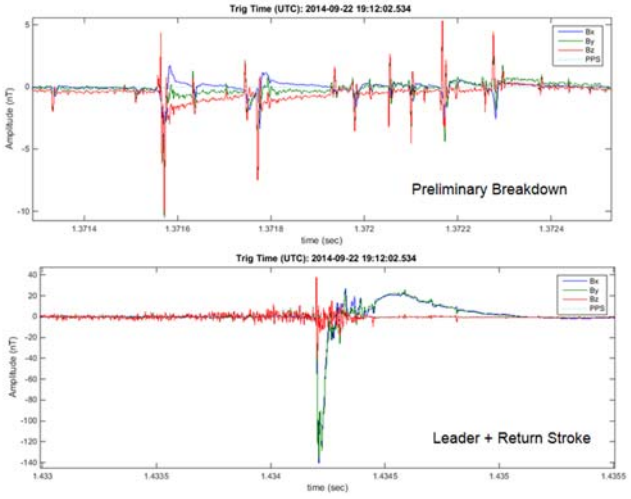

Fig. 8. Preliminary breakdown for case 1 CG flash.

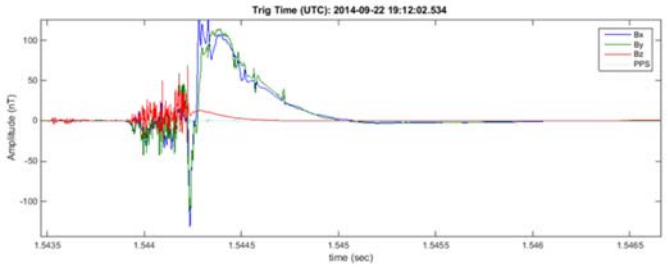

Fig. 9. Expanded view of magnetic field for RS 3 in case 1.

The ensuing sequence of ten "LDAR sources" shows that a leader was propagating upward to a height just below 14 km before turning toward the horizontal direction. The pattern is much like the downward negative leader prior to the 1st CG return stroke in the CG Case 1 above. During this (~50 ms) period, charge that had accumulated in these two "layers" (near 6 and 14 km) was "neutralized" in small horizontal regions of the cloud. The charge neutralization apparently caused local potential differences within the individual charge layers, which led to horizontal breakdown within the layers. What ensued throughout the rest of the flash, which lasted about 400 ms, were sequences of vertical charge transfer (breakdown followed by current flow) between layers and horizontal charge transfer within layers. The time color-coding of the source locations in the top (plan view) image shows that the initial breakdown occurred somewhat centrally within the overall flash, and then horizontal breakdown occurred repeatedly in multiple directions.

Fig. 12 shows the magnetic field waveforms (top plot) and the LDAR time/height evolution (lower plot) for the entire flash. An expanded view of the initial phase is shown in Fig. 13. The first pulse visible in Fig. 12 produced a much smaller B_z signal (the red trace) than the pulses that followed. This particular event resulted from a -87 kA CG stroke that occurred approximately 339 km to the west. The subsequent pulses that occurred during the initial phase of the flash

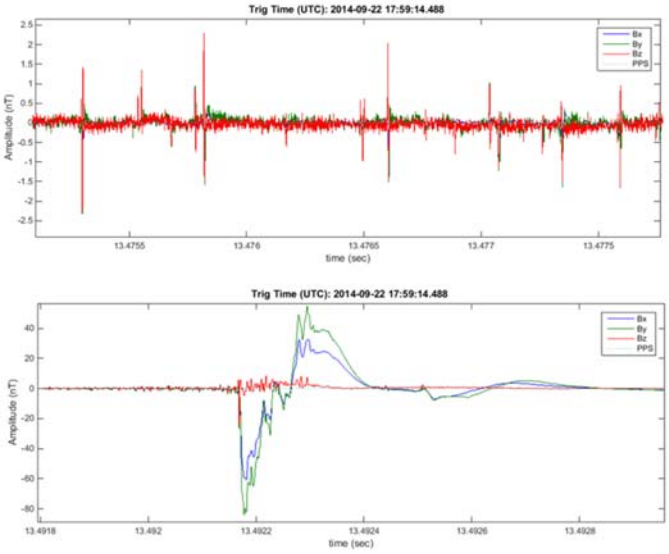

Fig. 10. Magnetic field data for case 2 CG flash.

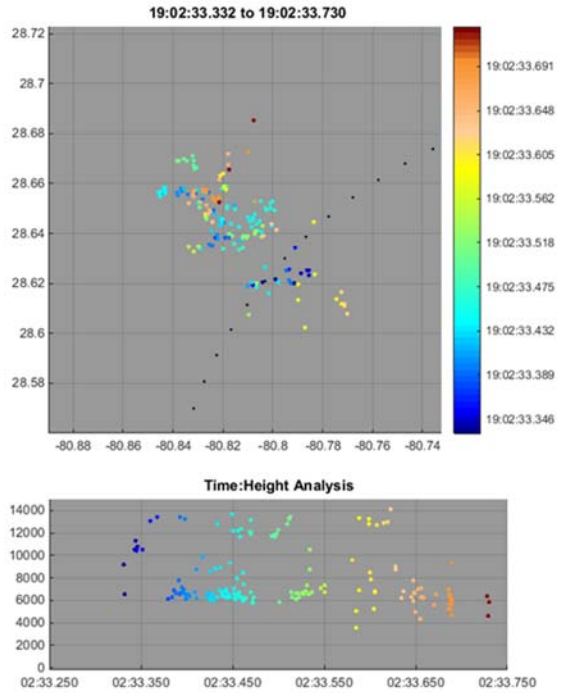

Fig. 11. LDAR data for IC flash.

(during the upward leader propagation from 6 to 14 km) produced relatively large B_z signals. Note also that the B_z signal gets "denser" (more pulses per unit time) when breakdown begins in the lower charge region at a height of 6 km starting at about 19:02:33.380 as shown in the LDAR plot. The B_z activity remains "dense" throughout the flash. One interpretation for this behavior is that the significant and brief horizontal currents that occurred during the cloud flash, as indicated by the LDAR sources within individual height layers, produce large transient vertical magnetic fields that were sensed by our B_z channel. These findings clearly indicate that there is useful information in vertical magnetic field waveforms.

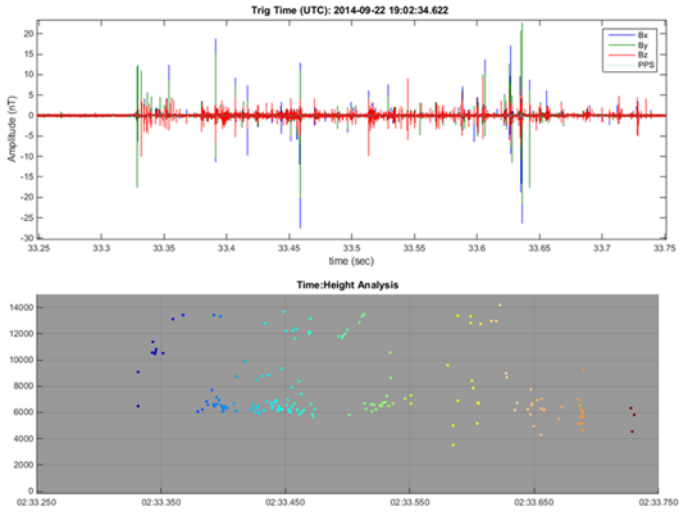

Fig. 12. Magnetic Field (top) and LDAR data (bottom) for IC flash.

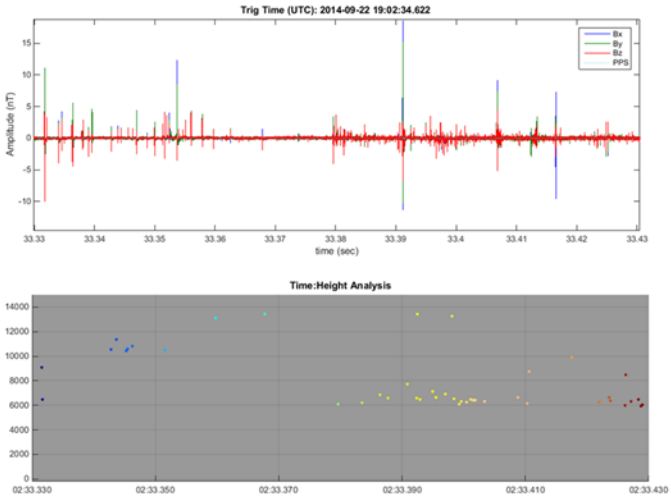

Fig. 13. Expanded view of the initial phase for the IC flash.

V. Conclusions

A six-axis sensor designed by QFS was used to record all six components of the electromagnetic radiation field from lightning processes associated with intra-cloud and cloud-to-ground lightning. The six-axis sensor can provide a 3-D direction to a source location using a Poynting vector calculation, and the accuracy of the direction provided depends primarily on the SNR of the detected electromagnetic radiation. A comparison of the sensor data and NLDN reports of cloud-to-ground lightning shows that the sensor produces amplitudes that are consistent with the transmission line model, and that it yields reasonably accurate horizontal directions (azimuth) to sources.

Measurements of the vertical (B_z) magnetic field associated with preliminary breakdown in clouds, near-ground stepped leaders, the early front of return-stroke waveforms, and the falling edge of return-stroke waveforms were presented. These processes were corroborated with LDAR data provided by NASA KSC. The strongest B_z signals were seen during the preliminary breakdown stage, although the signals during the stepped leader phase and the falling edge of the return stroke, when charge in branches is drained, showed relatively strong B_z signals as well. The B_z signal for some pulses was greater in amplitude than associated B_x or B_y signals. The data presented for the cloud flash show similar behavior; there were many pulses recorded in the B_z signal, and many were greater in amplitude than the associated B_x or B_y pulses.

Although some problems occurred during this initial step toward developing a stand-alone sensor that can provide direction information for lightning processes, the horizontal electric field and vertical magnetic field signals were sufficiently strong to record with a reasonable SNR. More data will be acquired in the future with a refined sensor that is calibrated such that 3-D directions can be determined using the Poynting vector calculation, and comparisons will be made with data from validated location systems in order to demonstrate the directional accuracy of the single station six-axis sensor.

Model-based estimates of location error indicate that near-ground height errors of less than 100 m might be achieved by using a 3-axis EB sensor capable of measuring the elevation angle, if at least one sensor is located within 10 km of the source location. This accuracy is not readily achievable using time-of-arrival geolocation methods.

Acknowledgment

This work was funded by NASA STTR NNX14CK08P. We are grateful for the assistance provided by Jennifer Wilson and Robert Brown of the Kennedy Space Center, who helped with the experimental setup and logistics.

References

Campos, L. Z. S., M. M. F. Sava, T. A. Warner, O. Pinto Jr., E. P. Krider, and R. E. Orville (2014), High-speed video observations of natural cloud-to-ground lightning leaders – A statistical analysis, Atmos. Res., Vol 135, doi:10.1016/j.atmosres.2012.12.011.

Cummins, K. L., and M. J. Murphy (2009), An overview of lightning locating systems: history, techniques, and data uses, with an in-depth look at the U.S. NLDN, IEEE Trans. on EMC, 51, 3, doi:10.1109/TEMC.2009.2023450.

Howard, J. S., M. A. Uman, C. J. Biagi, J. D. Hill, V. A. Rakov, D. M. Jordan (2011), Measured close lightning leader-step electric-field-derivative waveforms, J. Geophys. Res., 116(D8), doi:10.1029/2010JD015249.

International Telecommunication Union. Recommendation ITU-R P.372-11. Geneva, Switzerland, 2013.

International Telecommunication Union. Recommendation ITU-R P.372-8 . Geneva, Switzerland, 2003.

Nag, A. and V. A. Rakov (2009), Electric field pulse trains occuring prior to the first stroke in cloud-to-ground lightning, IEEE Trans. on EMC, Vol. 51, No. 1.

Nag. A., B. DeCarlo, and V. A. Rakov (2009), Analysis of microsecond- and submicrosecond-scale electric field pulses produced by cloud and ground lightning discharges, Atmos. Res., 91.

Stolzenberg, M., T. C. Marshall, S. Karunarathne, N. Karunarathne, T. A. Warner, R. E. Orville, and H.-D. Betz (2012), Strokes of upward illumination occurring within a few milliseconds after typical lightning return strokes, J. Geophys. Res Atmos., 117, D15, doi:10.1029/2012JD017654.

Thomson, E.M., P. Medelius, M. Rubinstein, M. A. Uman, J. Johnson, and J. W. Stone (1988), Horizontal electric fields from lightning return strokes, J. Geophys. Res., 93.

Thomas, R. J., P. R. Krehbiel, W. Rison, S. J. Hunyady, W. Winn, P. T. Hamlin, and J. Harlin (2004), Accuracy of the Lightning Mapping Array, J. Geophys. Res., 109, D14207.

Willett, J. C., J. C. Bailey, C. Leteinturier, and E. P. Krider (1990), Lightning electromagnetic radiation field spectra in the interval from 0.2 to 20 MHz, J. Geophys. Res. 100.